Deng *et al.*
Chinese Journal of Mechanical Engineering (2024) 37:85
https://doi.org/10.1186/s10033-024-01070-0

Chinese Journal of Mechanical Engineering

ORIGINAL ARTICLE

Open Access

Numerical Prediction of Ride Comfort of Tracked Vehicle Equipped with Novel Flexible Road Wheels

Yaoji Deng[1*], Zhiyue Wang[1], Youqun Zhao[2*], Junjie Gong[1], Hui Shen[1] and Fen Lin[2]

Abstract

Enhancing ride comfort has always constituted a crucial focus in the design and research of modern tracked vehicles, heavily reliant on the driving system's performance. While the road wheel is a key component of the driving system, traditional road wheels predominantly adopt a solid structure, exhibiting subpar adhesion performance and damping effects, thereby falling short of meeting the demands for high-speed, stable, and long-distance driving in tracked vehicles. Addressing this issue, this paper proposes a novel type of flexible road wheel (FRW) characterized by a catenary construction. The study investigates the ride comfort of tracked vehicles equipped with flexible road wheels by integrating finite element and vehicle dynamic. First, three-dimensional (3D) finite element (FE) models of both flexible and rigid road wheels are established, considering material and contact nonlinearities. These models are validated through a wheel radial loading test. Based on the validated FE model, the paper uncovers the relationship between load and radial deformation of the road wheel, forming the basis for a nonlinear mathematical model. Subsequently, a half-car model of a tracked vehicle with seven degrees of freedom is established using Newton's second law. A random road model, considering the track effect and employing white noise, is constructed. The study concludes by examining the ride comfort of tracked vehicles equipped with flexible and rigid road wheels under various speeds and road grades. The results demonstrate that, in comparison to the rigid road wheel (RRW), the flexible road wheel enhances the ride comfort of tracked vehicles on randomly uneven roads. This research provides a theoretical foundation for the implementation of flexible road wheels in tracked vehicles.

Keywords Ride comfort, Flexible road wheel, Finite element model, Dynamic model, Tracked vehicle

1 Introduction

Tracked vehicles are widely used in military, construction, forestry, mining, and agriculture, and the requirements for tracked vehicles are increasing. Optimal ride comfort has always been the main goal of modern tracked vehicle design and research [1, 2]. The performance of tracked vehicles is related to the engine and transmission systems; however, whether a vehicle can improve the average off-road speed and trafficability ultimately depends on the performance of the driving system [3–5]. When the buffer performance of the driving system or the adhesion between the road wheel and track is subpar, improving the average driving speed of the vehicle on off-road road terrain remains unattainable, even if the engine power is larger and the kilowatts per ton are higher. The road wheel is an important part of the driving system, but most road wheels adopt a rigid solid structure, and its structural characteristics determine that the adhesion performance and vibration reduction effect are poor and

*Correspondence:
Yaoji Deng
yjdeng@yzu.edu.cn
Youqun Zhao
yqzhao@nuaa.edu.cn
[1] College of Mechanical Engineering, Yangzhou University, Yangzhou 225127, China
[2] College of Energy and Power Engineering, Nanjing University of Aeronautics and Astronautics, Nanjing 210016, China

cannot meet the requirements of high-speed, stable, and long-term operation of tracked vehicles. This is one of the key bottlenecks that limit the further improvement of tracked vehicles.

Extensive research has been conducted on the structures and materials of road wheels. A variety of new materials, including aluminum alloy, composite armor, titanium alloy, improved armor, steel carbon fiber reinforced polymer, and others, have been employed to reduce the weight of weapons and equipment. This application aims to enhance the overall vehicle's lightweight characteristics and improve its mobility, thereby maximizing the battlefield survival and combat capability of tracked vehicles [6, 7]. In structural research, most scholars have proposed a variety of new configurations, combining road wheels and flexible road wheel (FRW) configurations, to improve the mobility, trafficability, and ride comfort of tracked vehicles [8]. Although these studies have achieved some beneficial results, they have not fundamentally broken through the bearing mechanism of traditional rigid road wheel (RRW), and the adhesion between the track and road has not been improved. Because only local areas of the road wheel participate in the loading, the loading efficiency is relatively low, and the adhesion performance is poor. Furthermore, the rigid track and rim exert pressure on the rubber in both directions, resulting in large deformation and a large amount of heat after rolling for a long time, which significantly affects the service life of the road wheel.

Considering the inherent shortcomings of traditional RRW, this study proposes a new type of composite FRW with a catenary structure. The stress in the FRW was more uniform, and the bearing capacity per unit mass was higher. The bottom rubber enables greater deformation in the radial direction, the average grounding pressure is reduced, and the adhesion between the road wheel and track and between the track and ground is improved, thereby improving the ride comfort, mobility, and trafficability of the tracked vehicle [9–11]. The mechanical characteristics of road wheels, which are an important part of the vibration transmission path, significantly affect the ride comfort of tracked vehicles. It is necessary to study the ride comfort of a tracked vehicle equipped with novel FRWs to provide a reference for replacing RRWs with FRWs to match tracked vehicles.

A tracked vehicle comprises a complex mechanical system. In particular, because of the existence of tracks, it is more difficult to describe the dynamic relationship between vehicles and the ground, and the service environments of tracked vehicles are very different, making them vulnerable to climatic conditions and other factors [12–14]. Historically, research on tracked vehicle performance has relied on experience and testing, following the traditional approach of "design, trial, production, test, and improvement" [15, 16]. This method is based on a large number of empirical formulas and experiments and has a long development cycle. In recent years, with the development and wide application of modeling and simulation technology, it has been applied in research on tracked vehicle performance [17–20]. For different types of tracked vehicles, various models are established to describe the stability, steering performance and passing performance of tracked vehicles [21–24].

To overcome the disadvantages of poor damping performance, poor adhesion, and heavy weight of traditional RRWs, a new FRW with a catenary construction was proposed in this study. The innovation of this study is to establish a nonlinear model of an FRW using the finite element method and numerically predict the ride comfort of a tracked vehicle equipped with FRWs combined with a half-vehicle dynamics model. Three-dimensional (3D) finite element (FE) models of the FRW and RRW considering the material and contact nonlinearities were established. The radial stiffness of the road wheel was analyzed to build a nonlinear wheel model. Subsequently, a half-car model of a tracked vehicle with seven degrees of freedom was established using Newton's second law and a random road model was constructed using white noise. Finally, the ride comfort of tracked vehicles equipped with FRW and RRWs at different speeds and road grades was studied by combining a nonlinear model of road wheels, half-car model, and random road model.

The specific chapters of this paper are organized as follows: Section 2 introduces the structure and finite element modeling of the FRW; the half-vehicle dynamic model of a tracked vehicle and road excitation model are described in Section 3; Section 4 presents the results of the simulation analysis; and a summary and prospects of the full paper are presented in Section 5.

2 Finite Element Modelling of FRW and RRW

2.1 Structure of FRW and RRW

Traditional RRWs are generally composed of four parts: A rim, spoke, and hub. Road wheels can be divided into three types according to the degree of vibration reduction: all-metal wheels (no vibration reduction), internal vibration reduction wheels, and external vibration reduction wheels (outer rubber ring). Among these, the external vibration-damping road wheel is the most widely used, and its rim is wrapped in a rubber apron.

The main functions of the road wheel are as follows: (1) Support the car body. This is the basic performance to ensure that the car body rolls on the track, and (2) to ease the impact. The road wheel tire is made of vulcanized rubber, which works together with the torsion bar spring and balance shaft to alleviate or absorb various impacts

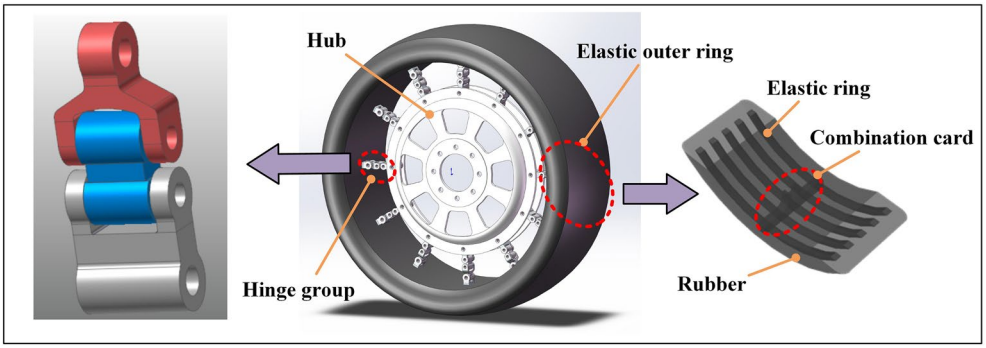

Figure 1 Structure of FRW

from the road surface, reducing the impact of various precision components on the car body and passengers. (3) Vibration isolation and noise reduction. Road wheel rolling on track. The uneven ground causes vibration. However, there will be vibrations between the road wheel and track, and at the same time, there will be impact and noise.

The overall requirements for road wheels are as follows: (1) To ensure minimum rolling resistance on the track, the rolling resistance can be reduced by reasonably designing the configuration, number, and size of the road wheels, appropriately increasing the rubber stiffness, and reducing the friction loss of the bearing. The purposes of the resistance are (2) long service life under various road conditions, (3) low dynamic load and noise, and (4) light weight.

In summary, the effect of road wheels on the performance of tracked vehicles is mainly reflected in the rolling resistance, ground pressure, maximum speed, lightweight, ride comfort, and heat dissipation. As the speed of tracked vehicles increases, the requirements for the road wheels also increase. Traditional road wheels have several shortcomings that limit further improvements in vehicle performance. Therefore, it is necessary to develop road wheels with new structures and cooperate with suspension systems to improve the mobility, passability, and ride comfort of tracked vehicles.

An FRW is a typical statically indeterminate structure, and its main structure includes a hinge group, elastic outer ring, and hub, as shown in Figure 1. The elastic outer ring is the main load-bearing part of the FRW and is composed of multiple sets of elastic rings, combination cards, and vulcanized rubber. A plurality of combination cards was evenly and equiangularly distributed along the circumference to lock the fixed elastic ring. Hinge groups are used to connect the elastic outer ring and hub and transfer the force and torque between them. The hinge group and combination card are connected by a pin shaft. Each hinge group is composed of two or three hinge bodies connected by pins such that the hinge group can bend freely under pressure and has a certain flexibility.

Ideally, the elastic outer ring, hub, and two hinge groups could form a statically indeterminate structure, whereas the remaining hinge groups could be regarded as additional constraints. The primary advantage of such a statically indeterminate structure lies in its operational resilience. If a portion of the hinge group experiences failure or damage, provided that it does not significantly impact the load-bearing capacity of the FRW, the remaining intact hinge components can continue to bear the load, ensuring the vehicle's continued operation. This feature significantly enhances the reliability and safety of the driving vehicle.

2.2 Finite Element Model

2.2.1 Three-Dimensional Geometrical Modeling

The geometric model of the FRW is assembled from individual parts, and the movement of the wheel is achieved by the interaction between the parts. Therefore, multiple coupling factors, including the structure of the parts, the connection and assembly relationship between the parts, and the force transmission, complicate the establishment of a finite element model of the FRW. To improve the efficiency of the modeling and solution, the structure of the FRW was reasonably simplified without affecting the function of each component. The complex hinge group was simplified into a three-link structure. The elastic ring wound with a steel wire was simplified into a ring with a rectangular cross-section. The load was assumed to be applied at the center of the wheel. The relative slip and contact between the elastic ring and rubber are ignored and considered as a whole. All the components of the FRW were built using the 3D modeling software CATIA.

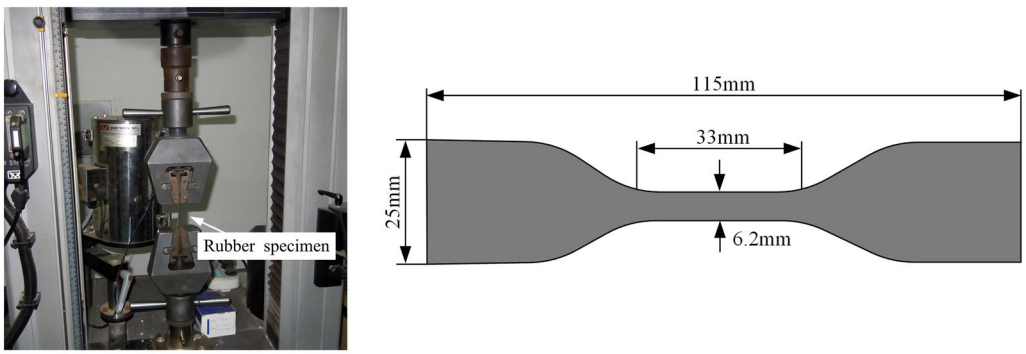

Figure 2 Uniaxial tensile test of rubber material: (**a**) Uniaxial tensile test, (**b**) Structure diagram of rubber specimen

2.2.2 Material Attribute Identification

The definition of material properties is an important part of the finite element modeling of FRW, which directly affects the accuracy of the simulation results. FRW materials are composed primarily of rubber and various metals. The properties of the rubber materials were obtained using a test method. The properties of the metal materials, including the Young's modulus, Poisson's ratio, and density, were provided by consulting the relevant literature or by the supplier.

Rubber is a superelastic material with clear viscoelastic characteristics and approximate volume incompressibility. Its mechanical properties exhibit high sensitivity to the environment, temperature, and load frequency, thus making the description of the complex behavior of rubber more difficult. At present, the commonly used and mature description methods of constitutive relationship of rubber materials mainly include statistical model based on molecular chain network and phenomenological model based on strain energy form [25–27]. However, most rubber constitutive relationships are described by phenomenological models based on the form of strain energy. The strain potential energy is used to describe the superelasticity of rubber materials; that is, the strain energy per unit reference volume stored in the material is defined as a function of the material strain at that point. The Mooney-Rivlin model, which has been widely used in engineering, satisfies the mechanical performance simulation of rubber materials. The typical binomial third-order expansion of its constitutive model can be expressed as:

$$W = C_{10}(I_1 - 3) + C_{01}(I_2 - 3). \tag{1}$$

The stress-strain relationship of the material constitutive model is defined as:

$$\frac{\sigma}{2(\lambda - \lambda^{-2})} = C_{10} + \frac{C_{01}}{\lambda}. \tag{2}$$

From Eq. (2), the relationship between $\frac{1}{\lambda}$ and $\frac{\sigma}{2(\lambda-\lambda^{-2})}$ is a straight line with slope C_{01} and intercept C_{10}. Rubber

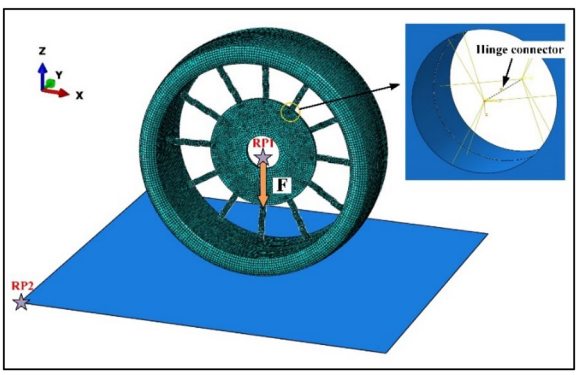

Figure 3 Finite element model of FRW with applied boundary conditions and loads

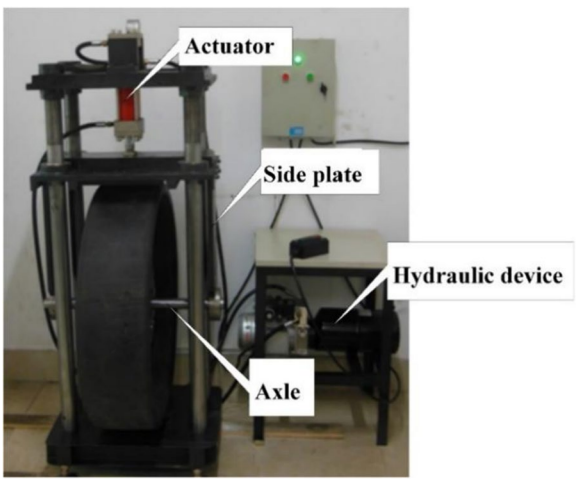

Figure 4 Road wheel test bench

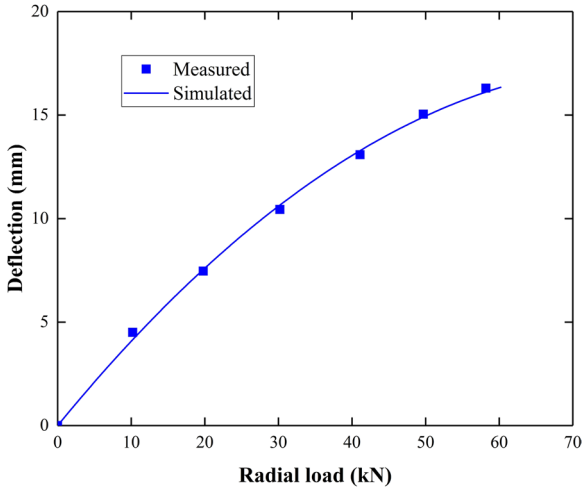

Figure 5 Verification results of radial deformation of the FRW

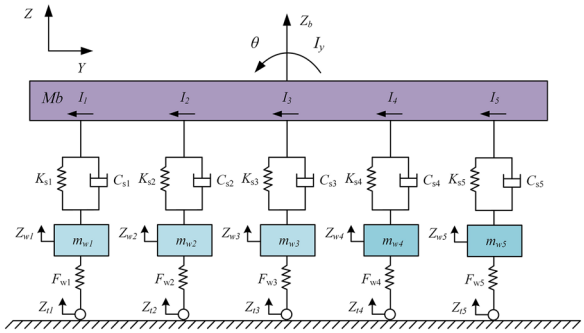

Figure 6 Dynamics model of half tracked vehicle with FRWs

material coefficients were determined by fitting the axial tensile test data.

The dumbbell-shaped test piece of the prepared rubber is shown in Figure 2(b), and the thickness of the test piece was 2 mm. The samples were fixed within the effective test range. To ensure the measurement accuracy, the measurement position was far from the clamping part. The loading speed of the tensile testing machine is set to 450 mm/min, and the test ambient temperature is controlled at 23 ℃±2 ℃. The test process is shown in Figure 2(a). After the test, the rubber test data were processed to obtain the stress-strain data of the rubber specimen, and parameter identification was performed according to Eq. (2), and two parameters of the Mooney–Rivlin constitutive model were obtained as follows: Three groups of tests were conducted, and the three groups of data were averaged to obtain the fitting results of the model parameters.

2.2.3 Meshing and Boundary Condition

The components of the FRW, such as the suspension hub, hinge group, and rubber layer, were all meshed using the solid element C3D8R, and the elastic ring embedded in the rubber layer was modeled using beam unit B31. The rotary effect between the hinge and hub or two hinges is simulated by connecting two reference points coupled to the inner surface of the pin bore using "hinge connector." The "hinged connector" only releases the rotational degrees of freedom between the two points while constraining the remaining five degrees of freedom. The elastic ring is embedded in rubber layer by "embedded element." The established finite element model of the FRW consists of 274257 elements and 327589 nodes.

The interaction between the FRW and road surface is divided into normal and tangential interactions. In

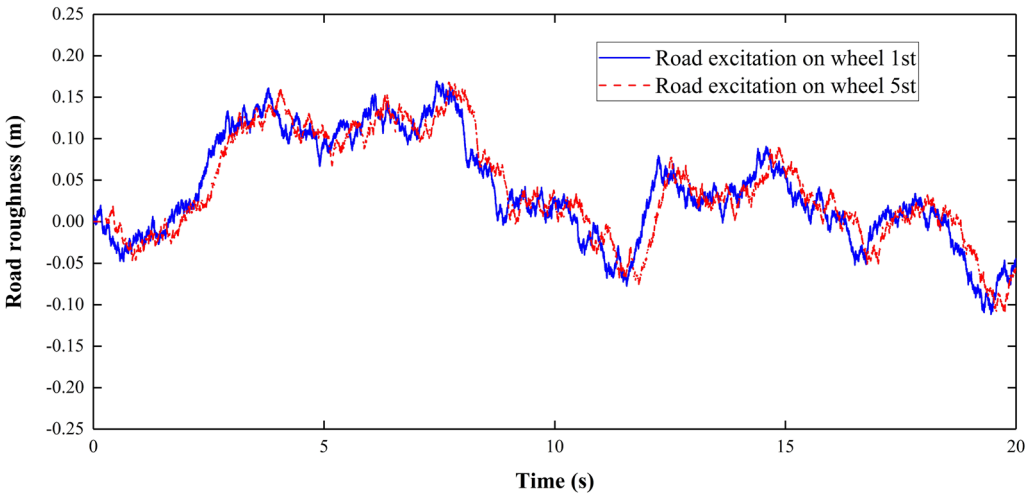

Figure 7 Road excitation applied to different road wheels

ABAQUS, the normal interaction of the contact interfaces is simulated using "hard contact" which defined that the contact pressure becomes zero or negative when they are separated and the corresponding node constraints fail. The penalty function method was used to determine the normal force, as expressed in Eq. (3).

$$f_1 = \begin{cases} K_n C & C \le 0, \\ 0 & C > 0. \end{cases} \tag{3}$$

The use of the small slip algorithm "surface to surface" can improve the accuracy of the stress calculation under the condition that the sliding between the contact surfaces is very less. The Coulomb friction model was used to determine the tangential force, as described in Eq. (4).

$$f_2 = \begin{cases} K_t \eta, & \text{Adhesive contact}, \\ \mu f_1, & \text{Sliding contact}. \end{cases} \tag{4}$$

Figure 3 shows the established finite element model of the FRW and the applied boundary conditions and loads. Compared with FRW, the deformation of the track is very small; therefore, it is set as a discrete rigid plane. A reference point RP2 was set on the analytical rigid plane, and three translational degrees of freedom and three rotational degrees of freedom in the x, y, and z directions were limited; thus, the rigid plane was completely fixed. A reference point RP1 coupled to the inner surface of the hub was set at the center of the hub; the translational degrees of freedom in the x and y directions and the rotational degrees of freedom in the x, y, and z directions were limited, and only the translational degrees of freedom in the z direction were released. Simultaneously, a gently loaded vertical force F is applied to reference point RP1 such that the FRW can only deform along the z-axis.

To facilitate a comparative analysis with the FRW, a three-dimensional finite element model of the RRW with the same dimensions as the FRW was established. The

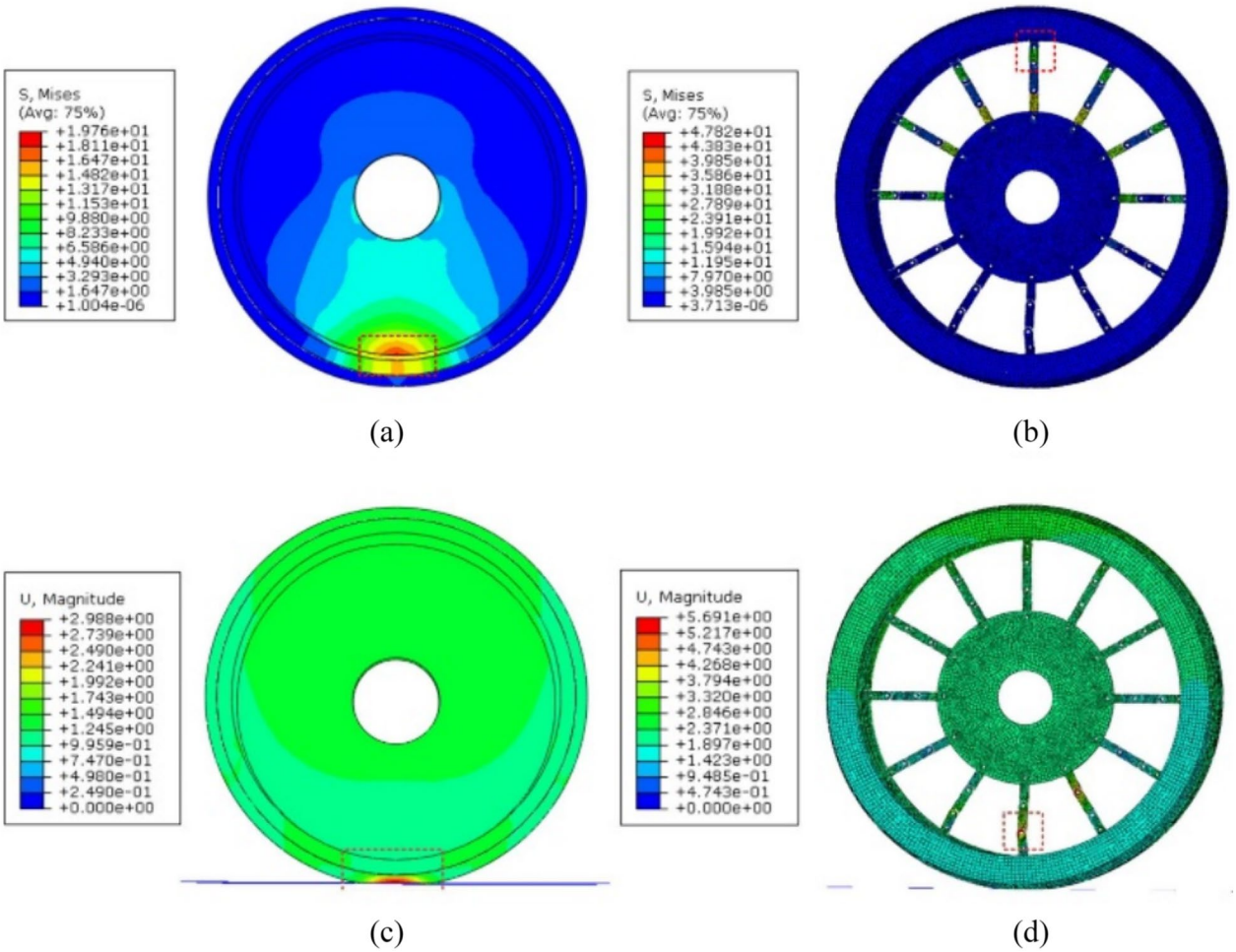

Figure 8 Comparison of stress and deformation between FRW and RRW under static load: (**a**) RRW stress, (**b**) FRW stress, (**c**) RRW deformation, (**d**) FRW deformation

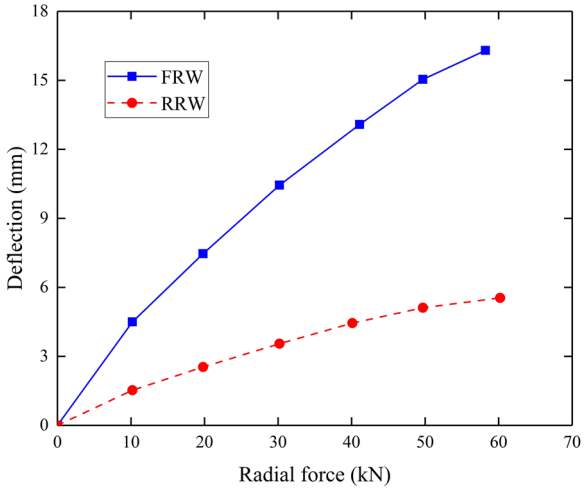

Figure 9 Radial deformation of FRW and RRW under different static load

meshing adopted a hexahedral mesh, and the material properties, boundary, and load condition settings were consistent with the static simulation parameters of the FRW.

2.3 Model Validation

The radial stiffness of a road wheel is a basic mechanical property of the road wheel and is affected by its structure and material. Using a self-developed wheel test bench, the deformation of the FRW under a static load was measured, and the experimental results were compared with the simulation results to verify the reliability and accuracy of the FE model.

The static loading test of an FRW test prototype was performed using a road wheel mechanical characteristic test bench independently developed by the research group. This bench is mainly composed of a power source, a hydraulic device, a control unit, and a rigid plate, as shown in Figure 4. The vertical load was gradually applied to the FRW to obtain the relationship between the vertical load and sinking amount of the FRW. The above steps were repeated to obtain the relationship between the vertical load and sinking amount of the FRW under different load conditions.

Figure 5 shows the variation curve of the radial load sinking of the FRW with the radial load. With an increase in the radial load, the sinking of the FRW increased nonlinearly. At the same time, the simulation results are in good agreement with the experimental results, and the relative error is no more than 5%.

3 Half Vehicle Model of the Tracked Vehicle WITH FRW

3.1 Dynamic Model of the Tracked Vehicle

A tracked vehicle is a complex nonlinear system with multiple degrees of freedom. If these dynamic relations are completely described, the dynamic model will be very complex, and the number of calculations will be large, which makes it difficult to meet the requirements of engineering applications. Therefore, it is necessary to simplify the tracked-vehicle model. The effect of complex road excitations is the main characteristic of tracked vehicles when driving off-road, and the vibration response is random. The assumptions and simplifications are as follows [28, 29]:

(1) The road surface on which tracked vehicles travel is rigid. The road roughness did not change because of the rolling of the wheels, and the roughness functions of the left and right ruts were the same. Road roughness only causes a time delay in the vibration input of each wheel.
(2) The track structure is regarded as an "infinite track" similar to the excitation of the paved ground, ignoring the effect of the track on the vehicle body, the road roughness with the wavelength less than the track pitch is completely covered by the track shoe.
(3) The center of mass of the vehicle body is symmetrical about the longitudinal axis. The rolling vibration of the vehicle body was low and soon stopped. The rolling vibrations of the vehicle body can be ignored. Only the vertical and pitching motions of the vehicle were considered. A dynamic model of the vehicle suspension system was established using a 7-DOF plane half-vehicle model.

Table 1 Fitting results of radial stiffness of the road wheel

Fitting Parameters	RRW		FRW	
SC	K_1=4.843×10^6	K_2=1.017×10^9	K_1=1.646×10^6	K_2=1.176×10^8
RSS	10.823		0.695	
RMS error	1.471		0.416	
Reduced Chi-Sqr	2.164		0.173	
Adj. R-square	0.998		0.999	

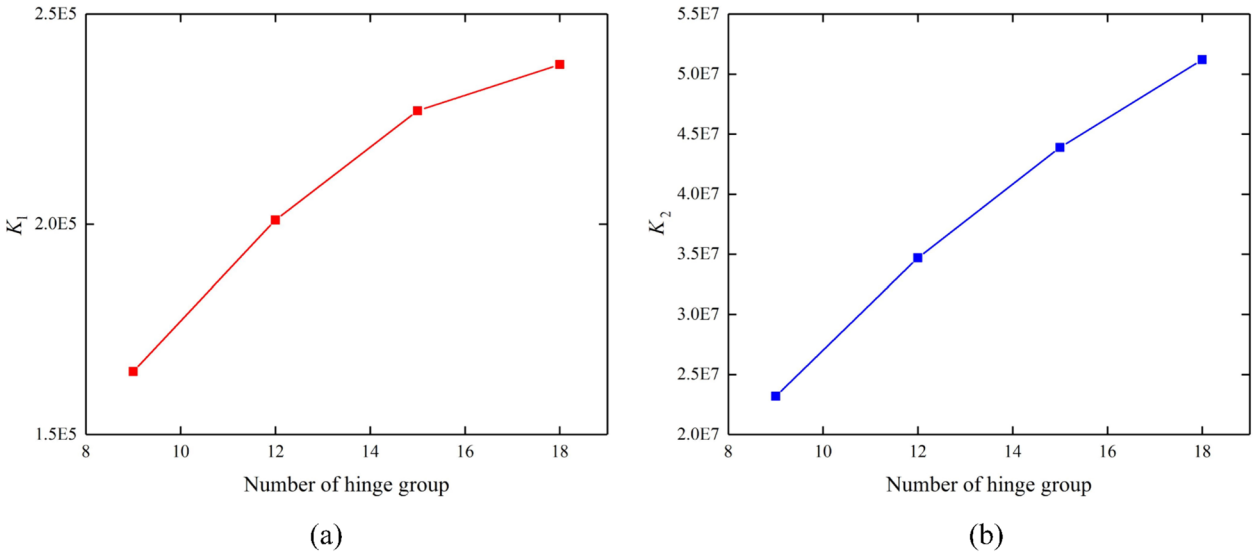

Figure 10 Stiffness coefficient varying with the number of hinge group: (**a**) K_1, (**b**) K_2

(4) The vehicle adopts an independent linear suspension that decomposes the suspension mass into sprung and unsprung masses.

(5) The damping force, elastic force, and gravity of the load wheel act on the center of mass of the load wheel.

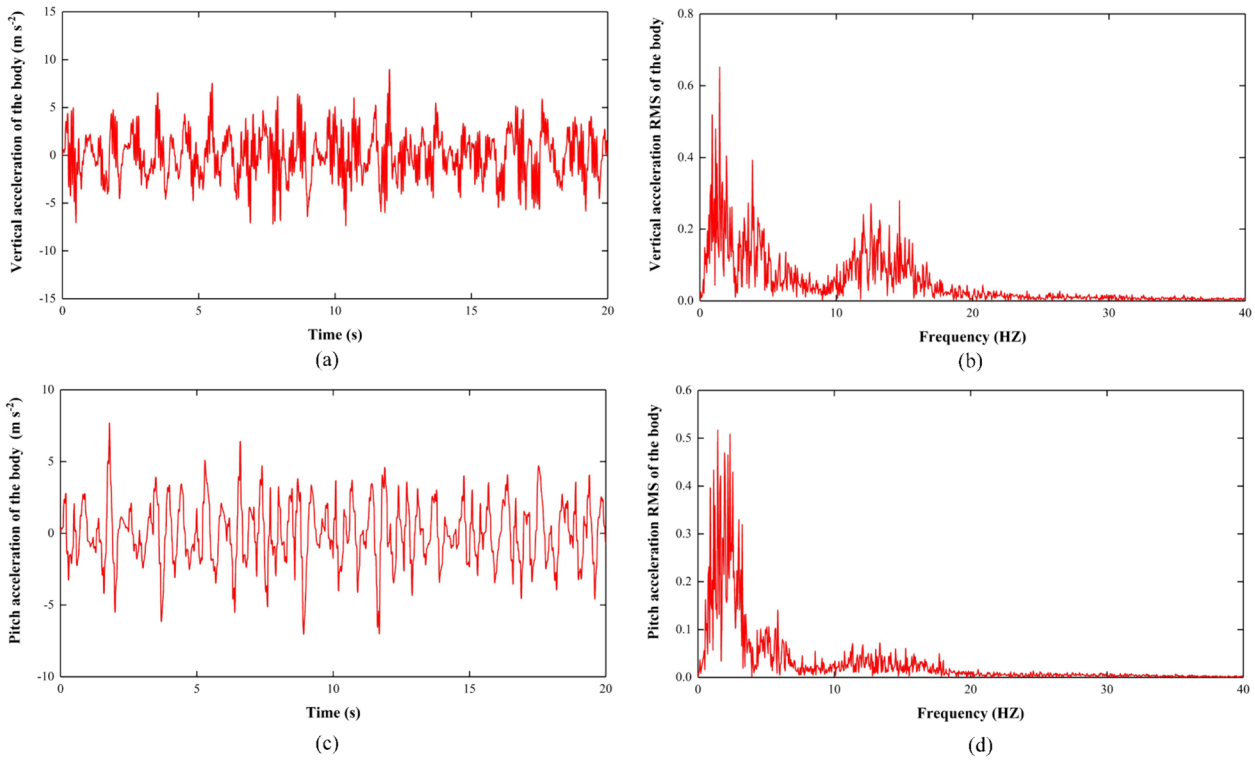

Figure 11 Dynamic response of the body: (**a**) Vertical acceleration, (**b**) RMS of vertical acceleration, (**c**) Pitch acceleration, (**d**) RMS of pitch acceleration

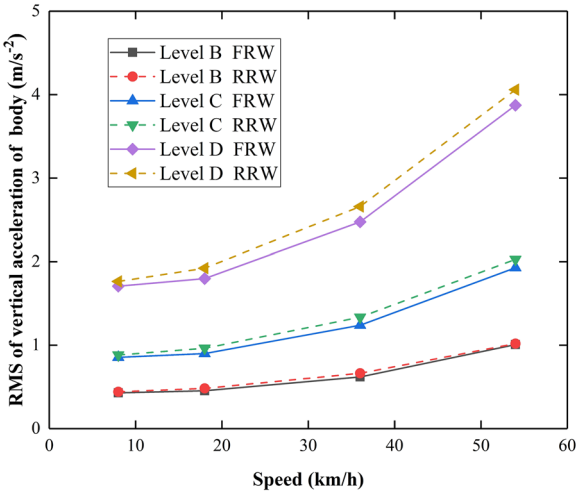

Figure 12 RMS of the vertical acceleration of the body varying with speed under different levels of road surfaces

The tracked vehicle traveled to the left at a constant speed. The centroid of the suspended mass at the static balance position of the tracked vehicle is selected as the origin of the dynamic coordinates. The longitudinal axis passing through the centroid of the tracked vehicle is X axis, the transverse X-axis is Y-axis, and Z-axis is Z axis. The pitch angular displacement of the transverse axis Y around the centroid of the vehicle body was θ, and the forward directions of X, Y, Z and θ were determined according to the right-hand rule. A simplified model of the semi-vehicle parametric dynamics of a tracked vehicle is shown in Figure 6. According to Newton's law of motion, the parameterized dynamic expression of a half-car is established as:

$$m_b\ddot{z}_b + \sum_{i=1}^{5} k_{si}(z_{bi} + l_i\theta - z_{wi}) + \sum_{i=1}^{5} c_{si}(\dot{z}_{bi} + l_i\dot{\theta} - \dot{z}_{wi}) = 0, \quad (5)$$

$$I\ddot{\theta} + \sum_{i=1}^{5} k_{si}l_i(z_{bi} + l_i\theta - z_{wi}) + \sum_{i=1}^{5} c_{si}l_i(\dot{z}_{bi} + l_i\dot{\theta} - \dot{z}_{wi}) = 0, \quad (6)$$

for $i = 1, \ldots, 5$.

All variables and parameters in the above expressions are listed in Ref. [15], which also states the typical values used in the simulations.

3.2 Road Excitation Considering the Track Effect

The vibration sources varied while the tracked vehicle was running. The vibration in the vehicle body is primarily due to the vibration of the engine, and the main source of the vehicle body vibration is the input of the road excitation. Road excitations can be divided into two main types. Discrete excitation occurs when a tracked vehicle encounters bulges or pits while driving. When tracked vehicles encounter continuous uneven road excitations while driving, these are called random excitations. In this study, a road-surface excitation model was established using a random road input.

When a tracked vehicle encounters a randomly excited road surface, the road surface roughness must be used before the road input model is established. The road surface roughness curve indicates the relative changes in the road surface and reference plane displacement. The relative change in the vertical displacement of a vehicle while driving can be defined using a spectral density function. When the speed of the tracked vehicle is constant, a conversion between the time and space frequencies can be realized, and the time frequency can be used instead of the space frequency. Combined with relevant international standard documents, the spectral density of road roughness was fitted using the following expression [30]:

$$G_q(n) = G_q(n_0)\left(\frac{n}{n_0}\right)^{-w}. \quad (8)$$

The road roughness was divided into eight levels according to the difference in power spectral density, the road roughness is divided into 8 levels. Because the road wheel of the tracked vehicle acts on the track, it acts as a filter for the ground excitation input, which can filter out uneven road excitations of small wavelengths. The input models for the road surface can be divided into two categories: integrated and filtered white noise.

$$m_{wi}\ddot{z}_{wi} - k_{si}(z_b + l_i\theta - z_{wi}) - c_{si}(\dot{z}_b + l_i\dot{\theta} - \dot{z}_{wi}) + k_1(z_{wi} - z_{ti}) + k_2(z_{wi} - z_{ti})^2 = 0, \quad (7)$$

Table 2 RMS of the vertical acceleration of the body under different speed and road levels

Speed (km/h)	B grade			C grade			D grade		
	FRW	RRW	Change (%)	FRW	RRW	Change (%)	FRW	RRW	Change (%)
8	0.43	0.44	− 3.17	0.86	0.88	− 3.17	1.71	1.76	− 3.23
18	0.45	0.48	− 6.00	0.90	0.96	− 6.64	1.80	1.92	− 6.50
36	0.62	0.66	− 6.64	1.24	1.34	− 7.26	2.48	2.66	− 6.88
54	1.01	1.02	− 1.18	1.93	2.03	− 5.00	3.87	4.06	− 4.58

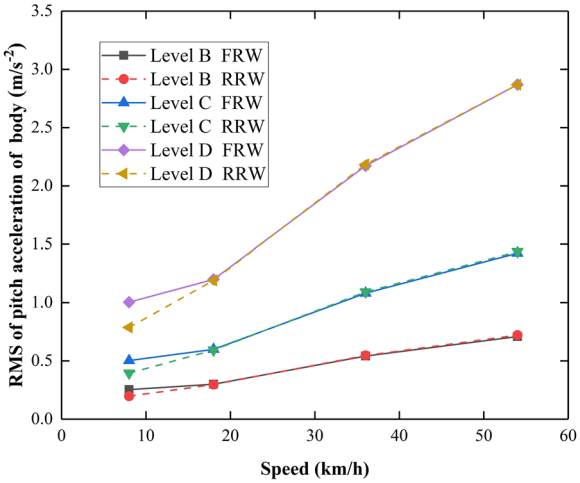

Figure 13 RMS of pitching acceleration of vehicle body varying with vehicle speed under different road grades

However, integrated white noise cannot reflect the actual situation of road unevenness very well, whereas filtered white noise can consider the filter effect of the track and achieve good results. White noise is selected as the input model for the road surface. The input of the road excitation to the road wheels is [31]:

$$\dot{z}_i = -2\pi f_0 z_i + 2\pi\sqrt{G_0 u}\omega(t). \tag{9}$$

The simulation results of the road input obtained according to Eq. (9) is illustrated in Figure 7. It can be seen from the figure that the maximum height of the road displacement can reach 0.15 m, and there is a delay between the first and fifth road wheels, which is in line with the real situation encountered during the operation of tracked vehicles.

4 Results Analysis and Discussion

4.1 Radial Stiffness Analysis of FRW and RRW

The mechanical characteristics of the road wheel determine many important properties of a tracked vehicle, and its stiffness characteristics have a significant effect on vehicle performance. The radial stiffness of road wheels directly affects the ride comfort of tracked vehicles.

Based on the established nonlinear finite element model of the FRW, the static load-bearing conditions of the road wheels and factors affecting the radial stiffness were analyzed in detail. Simultaneously, the simulation results of the FRW and RRW were compared to provide data for the subsequent establishment of the nonlinear stiffness model.

Figure 8 shows a comparison of the overall stress and deformation distributions of RRW and FRW under a vertical load of 30 kN. As shown in Figure 8(a), the high-stress area was located at the bottom of the RRW and extended to the surroundings, verifying the bottom load-bearing mode of the RRW. The high-stress area of the FRW is located on the upper hinge group, and the closer the hinge group is to the central axis, the greater the stress, as shown in Figure 8(b). As shown in Figure 8(c), the maximum deformation of RRW occurred at the bottom rubber part. Compared with the RRW, the overall deformation of the FRW was larger, and the deformation distribution was more uniform, as shown in Figure 8(d).

Figure 9 shows the radial deformations of FRW and RRW under different static loads. The results show that the radial deformation of the FRW is much greater than that of the RRW, indicating that the flexible road wheel is softer.

The linear wheel model was first used in the analysis of vehicle dynamics; however, it has been proven that this assumption is inaccurate. Therefore, it is necessary to develop a more accurate nonlinear model based on the linear model. In engineering applications, the elastic and damping forces of a road wheel are precisely given by Eqs. (10) and (11):

$$F_w = K_1 x + K_2 x^2, \tag{10}$$

$$F_c = C_w x. \tag{11}$$

This model has simple and clear features that satisfy the requirements of vehicle dynamics analysis. Therefore, this model was used in this study to analyze the ride comfort of a tracked vehicle.

Based on the established nonlinear finite element model of the FRW and RRW, the relationship between the deformation and radial load was obtained numerically, and the stiffness coefficient (SC) K_1 and K_2 were obtained by fitting the load-deflection curve using the Least Squares method. To evaluate the goodness of fit of

Table 3 RMS of the pitching acceleration of the body under different speed and road levels

Speed (km/h)	B grade			C grade			D grade		
	FRW	RRW	Change (%)	FRW	RRW	Change (%)	FRW	RRW	Change (%)
8	0.25	0.20	28.93	0.50	0.40	27.34	1.00	0.79	27.57
18	0.30	0.29	1.01	0.60	0.59	1.01	1.20	1.19	0.76
36	0.54	0.55	− 0.91	1.08	1.09	− 1.01	2.17	2.184	− 0.55

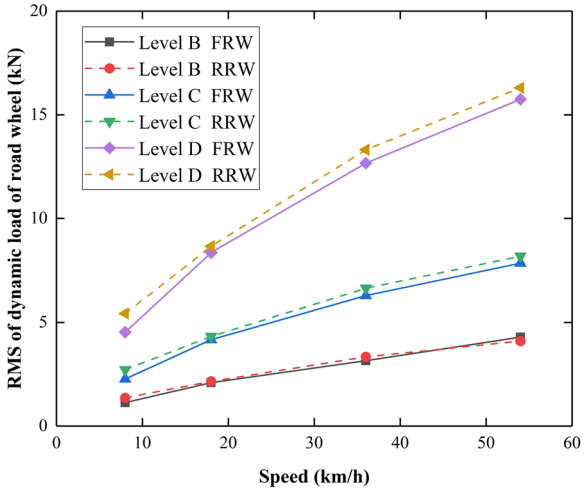

Figure 14 RMS of dynamic load of FRW and RRW varying with vehicle speed under different road grades

the fitted curve, multiple indicators such as the residual sum of squares (RSS), root mean square error, reduced Chi-Sqr, and R-squared were used. The smaller the residual sum of squares, root mean square error, and reduced Chi-Sqr in the indicators, the better the fit; the closer the R-square is to 1, the more consistent the regression expression is with the observed value. The parameters of the final fitted regression expression and evaluation index are listed in Table 1. These parameters indicated that the curve fit well.

The number of hinge groups is an important design parameter that significantly affects the mechanical properties of FRW. A finite element model of an FRW with different numbers of hinge groups was established, the static bearing performance was simulated to obtain the relationship between the deformation and load, and the stiffness coefficient was obtained by quadratic polynomial fitting. Figure 10 shows the influence of the number of hinge groups on stiffness coefficients K_1 and K_2. As shown in the figure, stiffness coefficients K_1 and K_2 increase with an increase in the number of hinge groups.

4.2 Dynamic Response of Tracked Vehicles with FRWs

The fitted nonlinear model of FRWs was added to the semi-vehicle dynamic model of a tracked vehicle for ride comfort simulation analysis. Considering the most frequent driving conditions of tracked vehicles, a grade D road was selected in the simulation, and the speed was set to 36 km/h.

Figure 11(a) shows the vertical acceleration of the vehicle body in the time domain. As shown in the figure, the maximum vertical acceleration of the vehicle body was approximately 10 m/s^2. Figure 11(b) shows the root mean square (RMS) of the vertical acceleration amplitude of the vehicle body in the frequency domain. It can be clearly seen from the figure that there are three resonance peaks in the vertical acceleration of the vehicle body, which occur at frequencies of approximately 1.65 Hz, 3.97 Hz and 13.89 Hz respectively, and the resonance peak decreases with the increase in frequency.

Figure 11(c) shows the pitch acceleration of the vehicle body in the time domain. It can be seen from the figure that the maximum value of pitching acceleration of the vehicle body is about 7.8 m/s^2. Figure 11(d) shows the root mean square of the pitching acceleration amplitude of the vehicle body in the frequency domain. It can be observed from the figure that there are two obvious resonance peaks of pitch acceleration, and the corresponding frequencies are 1.36 Hz and 5.89 Hz respectively.

4.3 Comparative Analysis on Ride Comfort of Tracked Vehicles with RRWs and FRWs

To evaluate the ride comfort of tracked vehicles with flexible road wheels, the vertical acceleration, pitching acceleration, and root mean square of the dynamic load of the road wheel were used as evaluation indices to compare and analyze the ride comfort of tracked vehicles with rigid and flexible road wheels at different speeds and road grades.

Figure 12 and Table 2 show the root mean square of the vertical acceleration of a vehicle body equipped with rigid

Table 4 RMS of the dynamic load under different speed and road levels

Speed (km/h)	B grade			C grade			D grade		
	FRW	RRW	Change (%)	FRW	RRW	Change (%)	FRW	RRW	Change (%)
8	1.13	1.36	− 16.69	2.27	2.72	− 16.62	4.53	5.43	− 16.52
18	2.10	2.16	− 2.96	4.17	4.32	− 3.59	8.36	8.66	− 3.49
36	3.15	3.34	− 5.60	6.30	6.65	− 5.37	12.67	13.31	− 4.85
54	4.29	4.10	4.66	7.86	8.19	− 4.07	15.75	16.30	− 3.41

and flexible road wheels, varying with the vehicle speed on different road grades. It can be observed from the figure and table that with an increase in the vehicle speed and road level, the root mean square of the vertical acceleration of the vehicle body also increases. The root mean square of the vertical acceleration of the vehicle body with RRWs was greater than that of the vehicle body with FRWs. With an improvement in vehicle speed, the difference between them first increased and then decreased; however, the road grade had little effect.

Figure 13 and Table 3 show the root mean square of the pitch acceleration of the vehicle body equipped with rigid and flexible road wheels as a function of the vehicle speed on different road grades. It can be observed from the figure and table that with an increase in the vehicle speed and road level, the root mean square of the pitch acceleration of the vehicle body also increases. When the vehicle speed was low (8 km/h), the root mean square of the pitch acceleration of the vehicle body equipped with RRWs was approximately 28% lower than that of the vehicle body equipped with FRWs. With an improvement in road grade, the difference between the two tends to decrease. However, when the vehicle speed more than 18 km/h, the gap between the two became very small.

Figure 14 and Table 4 show that the root mean square of the average dynamic load of the rigid and flexible road wheels varies with the vehicle speed on different road grades. It can be observed from the figure and table that with an increase in the vehicle speed and road grade, the root mean square of the dynamic load of the road wheel also increases. The root mean square of the dynamic load of RRW was larger than that of FRW. With an improvement in road grade, the difference between the two tends to increase. However, with an increase in vehicle speed, the difference between the two first decreases and then increases.

5 Conclusions

(1) Considering the drawbacks of traditional RRW, such as low bearing efficiency, heavy weight, and poor vibration reduction, this study proposes a new type of flexible road wheel that breaks through the solid structure of the traditional RRW, adopting a flexible catenary structure.

(2) A three-dimensional finite element model of the FRW considering material and contact nonlinearity was established using the nonlinear finite element analysis software ABAQUS. The reliability and accuracy of the established finite element model for the FRW were verified using a self-developed wheel-test bench.

(3) The overall stress–strain and radial stiffness of the FRW were analyzed, calculated, and compared with the static finite element analysis results of the RRW. The research results show that, compared with RRW, the overall deformation of FRW is more reasonable and uniform, and the radial stiffness is smaller. Nonlinear models of FRW and RRW were established by fitting the finite element analysis results.

(4) The ride comfort of tracked vehicles with FRWs and RRWs was compared and analyzed. The results show that FRWs can effectively reduce the vertical acceleration of the vehicle body and the dynamic load of the road wheels compared with RRWs, and the cushioning effect is more obvious with an improvement in road grade. The results provide a foundation for replacing RRWs with FRWs and matching tracked vehicles.

(5) This study investigated the influence of FRW on the ride comfort of tracked vehicles and showed that FRW are beneficial for improving the ride comfort of tracked vehicles. However, to apply FRW to tracked vehicles, the comprehensive performance of tracked vehicles with FRWs, including their trafficability, mobility, and stability, must be further verified.

Acknowledgements
Not applicable.

Authors' Contributions
YD performed the simulations and wrote the manuscript. ZW and FL provided the numerical model and program. YZ provided guidance on the design of cases. HS and JG modified the manuscript to improve the presentation. All authors read and approved the final manuscript.

Funding
Supported by National Natural Science Foundation of China (Grant No. 11672127), Innovative Science and Technology Platform Project of Cooperation between Yangzhou City and Yangzhou University of China (Grant No. YZ2020266), Advance Research Special Technology Project of Army Equipment of China (Grant No. AGA19001), Innovation Fund Project of China Aerospace 1st Academy (Grant No. CHC20001), Fundamental Research Funds for the Central Universities of China (Grant No. NP2022408), Jiangsu Provincial Postgraduate Research & Practice Innovation Program of China (Grant No. SJCX23_1903).

Data availability
The data that support the findings of this study are available from the corresponding author, upon reasonable request.

Declarations

Competing Interests
The authors declare no competing financial interests.

Received: 22 March 2022 Revised: 4 July 2024 Accepted: 8 July 2024
Published online: 02 August 2024

References

[1] V Randive, S C Subramanian, A Thondiyath. Design and analysis of a hybrid electric powertrain for military tracked vehicles. *Energy*, 2021, 229: 120768.

[2] I Mahalingam, C Padmanabhan. A novel alternate multibody model for the longitudinal and ride dynamics of a tracked vehicle. *Vehicle System Dynamics*, 2019, 59(3): 433–457.

[3] M Yamada, G Yamauchi, T Hashimoto. Fundamental study on underwater trafficability for tracked vehicle. *Journal of Terramechanics*, 2021, 98: 42–49.

[4] Y Q Xia, M Y Fu, C M Li, et al. Active disturbance rejection control for active suspension system of tracked vehicles with gun. *IEEE Transactions on Industrial Electronics*, 2018, 65(5): 4051–4060.

[5] P X Wang, X T Rui, H L Yu. Study on dynamic track tension control for high-speed tracked vehicles. *Mechanical Systems and Signal Processing*, 2019, 132(1): 277–292.

[6] Y J Deng, Y Q Zhao, H Xu, et al. Rigid-flexible coupling modelling and dynamic performance analysis of novel flexible road wheel. *Proceedings of the Institution of Mechanical Engineers, Part K: Journal of Multi-Body Dynamics*, 2020, 234(1): 67–81.

[7] J H Kim, S M Park, J J Lee, et al. A study on flow forming process of magnesium road wheel. *Transactions of Materials Processing*, 2014, 23(2): 116–121.

[8] B J Yan, D G Sun, Y Song, et al. Stress-deformation-temperature behavior of a rolling segmented constrained layer damped bogie wheel. *Noise Control Engineering Journal*, 2012, 60(6): 655–664.

[9] Y J Deng, Y Q Zhao, F Lin, et al. Simulation of steady-state rolling non-pneumatic mechanical elastic wheel using finite element method. *Simulation Modelling Practice and Theory*, 2018, 85: 60–79.

[10] Y J Deng, Y Q Zhao, F Lin, et al. Influence of structure and material on the vibration modal characteristics of novel combined flexible road wheel. *Defence Technology*, 2022, 18(7): 1179–1189.

[11] Q W Wang, Y Q Zhao, H Xu, et al. Adaptive backstepping control with grey signal predictor for nonlinear active suspension system matching mechanical elastic wheel. *Mechanical Systems & Signal Processing*, 2019, 131: 97–111.

[12] N Strawa, D I Ignatyev, A C Zolotas, et al. On-line learning and updating unmanned tracked vehicle dynamics. *Electronics*, 2021, 10(2): 187.

[13] P X Wang, G P Wang, X T Rui, et al. Contact dynamics analysis of the single-pin meshing pair of a tracked vehicle. *Nonlinear Dynamics*, 2021, 104(2): 1139–1155.

[14] A A Abyzov, I I Berezin. FEM simulation of tracks with soil interaction in curvilinear motion of tracked vehicle. *Lecture Notes in Mechanical Engineering*, 2021: 736–743.

[15] A Dhir, S Sankar. Ride dynamics of high-speed tracked vehicles: Simulation with field validation. *Vehicle System Dynamics*, 1994, 23: 379–409.

[16] Y F Miao, G P Wang, X T Rui. Dynamics modeling, simulation, and optimization of vibration characteristics of the tracked vehicle system. *Journal of Vibration & Control*, 2021, 27(21): 2451–2465.

[17] Z D Ma, N C Perkins. A super-element of track-wheel-terrain interaction for dynamic simulation of tracked vehicles. *Multibody System Dynamics*, 2006, 15(4): 347–368.

[18] A Nicolini, F Mocera, A Soma. Multibody simulation of a tracked vehicle with deformable ground contact model. *Proceedings of the Institution of Mechanical Engineers, Part K: Journal of Multi-Body Dynamics*, 2019, 233(1): 152–162.

[19] A Jakati, S Banerjee, C Jebaraj. Development of mathematical models, simulating vibration control of tracked vehicle weapon dynamics. *Defence Science Journal*, 2017, 67: 465–475.

[20] M A Subari, K Hudha, Z A Kadir, et al. Development of path tracking control of a tracked vehicle for an unmanned ground vehicle. *International Journal of Advanced Mechatronic Systems*, 2020, 8(4): 136–142.

[21] W G Ata, S O Oyadiji. An investigation into the effect of suspension configurations on the performance of tracked vehicles traversing bump Terrains. *Vehicle System Dynamics*, 2014, 52(7): 969–991.

[22] W G Ata, A M Salem, Semi-active control of tracked vehicle suspension incorporating magnetorheological dampers. *Vehicle System Dynamics*, 2017, 55(5): 626–647.

[23] P X Wang, X T Rui, H L Yu, et al. Dynamics modeling and control of active track tensioning system for tracked vehicle. *Journal of Vibration & Control*, 2019, 26(11–12): 989–1000.

[24] N Tomasz, J Andrzej, K Janusz. Modeling verification of an advanced torsional spring for tracked vehicle suspension in 2S1 vehicle model. *Engineering Structures*, 2021, 229: 111623.

[25] Y J Deng, Y Q Zhao, M M Zhu, et al. Comparative analysis of static loading performance of rigid and flexible road wheel based on finite element method. *Defence Science Journal*, 2020, 70(1): 41–46.

[26] B Mashadi, S Ebrahimi-Nejad, M Abbaspour. A rolling resistance estimate using nonlinear finite element numerical analysis of a full three-dimensional tyre model. *Proceedings of the Institution of Mechanical Engineers, Part D: Journal of Automobile Engineering*, 2019, 233(1): 147–160.

[27] C F Wei, O A Olatunbosun. The effects of tyre material and structure properties on relaxation length using finite element method. *Materials & Design*, 2016, 102: 14–20.

[28] H X Yang, X M Xu, J C Hong. Automatic parking path planning of tracked vehicle based on improved A* and DWA algorithms. *IEEE Transactions on Transportation Electrification*, 2023, 9(1): 283–292.

[29] R Li, J J Fan, Z D Han, et al. Configuration design and control of hybrid tracked vehicle with three planetary gear sets. *Journal of Central South University*, 2021, 28(7): 2105–2119.

[30] S Türkay, H Akcay. A study of random vibration characteristics of the quarter-car model. *Journal of Sound & Vibration*, 2005, 282(1–2): 111–124

[31] Y J Deng, Y Q Zhao, W Pi, et al. The influence of nonlinear stiffness of novel flexible road wheel on ride comfort of tracked vehicle traversing random uneven road. *IEEE Access*, 2019, 7: 165293–165302.

Yaoji Deng born in 1991, is currently a lecturer at *College of Mechanical Engineering, Yangzhou University, China*. He received his doctorate degree from *Nanjing University of Aeronautics and Astronautics, China*, in 2020. His research interests include safety explosion-proof tire and intelligent vehicle.

Zhiyue Wang born in 1998, is currently a master candidate at *Yangzhou University, China*. He received his bachelor degree in mechatronic engineering from *Wuxi Taihu University, China*, in 2021.

Youqun Zhao born in 1968, is currently a professor at *College of Energy and Power Engineering, Nanjing University of Aeronautics and Astronautics, China*.

Junjie Gong born in 1969, is currently a professor at *College of Mechanical Engineering, Yangzhou University, China*.

Hui Shen born in 1969, is currently a professor at *College of Mechanical Engineering, Yangzhou University, China*.

Fen Lin born in 1980, is currently an associate professor at *College of Energy and Power Engineering, Nanjing University of Aeronautics and Astronautics, China*.